Quaternary Science Reviews 345 (2024) 109011

Contents lists available at ScienceDirect

Quaternary Science Reviews

journal homepage: www.elsevier.com/locate/quascirev

Deep north atlantic circulation strength: Glacial-interglacial variability over the last 400,000 years

N. Stevenard [a,b,*], C. Kissel [a], A. Govin [a], C. Wandres [a]

[a] Laboratoire des Sciences du Climat et de l'Environnement, LSCE/IPSL, CEA-CNRS-UVSQ, Université Paris-Saclay, Gif-sur-Yvette, France
[b] Université Grenoble Alpes, CNRS, IRD, Grenoble INP, IGE, Grenoble, France

ARTICLE INFO

Handling editor: A. Voelker

Keywords:
Pleistocene
Paleoceanography
Paleoclimatology
North Atlantic
Deep ocean circulation

ABSTRACT

Most of the high-resolution studies investigating the past variability of the deep North Atlantic circulation are focused on recent timescales, but little is known for periods older than the last glacial period. Based on magnetic, elemental and physical grain-size proxies of three pairs of sediment cores located South of Iceland, we reconstructed the past changes in grain-size and basaltic-derived grain concentration over the last 400 ka (1 ka = 1000 years). The source and grain-size proxies exhibit highly similar variations between the three sites, suggesting they are affected by the same regional process. Persistently lower concentrations and finer grain-sizes recorded in the southernmost and deeper site compared to the northern sites indicate a North to South gradient that is consistent with the southward transport of sediments from a northern basaltic source by a deep current. Therefore, we interpret changes recorded by the ensemble of proxies at the three sites as past variations in the ISOW intensity. These new results show persistent influence, over the entire 400 ka, of a southward deep-water flow in the subpolar North Atlantic, from 1800 to 2800 m water depth. The "off mode" of deep Atlantic circulation during Heinrich events suggested by many studies is therefore questioned. This study extends the previous observations made for the 20–65 ka period over the last 400 ka. Our results also show that the three studied sites are bathed by a deep-water mass formed in the Nordic Seas, during both glacial and interglacial periods, suggesting that the present-day convection areas were still active during glacial periods. Our ISOW intensity records are highly similar to those of deep-water ventilation. We propose that the strength of overflows in the North Atlantic regulates the volume of North Atlantic Deep Water (NADW) and its southward transport in the Atlantic basin. Therefore, the Southern source waters may only act as an opportunistic component of the deep Atlantic circulation, invading or retreating depending on the NADW strength.

1. Introduction

Ocean circulation plays a crucial role in the climate system by exchanging heat and moisture with the atmosphere and storing (or releasing) greenhouse gases in (from) its deeper parts. In this context, over the past few decades, many studies focused on reconstructing the past variability of the Atlantic Meridional Overturning Circulation (AMOC) in order to better understand climate-ocean interactions (Broecker and Denton, 1990; McManus et al., 1999; Rahmstorf, 2002; Thornalley et al., 2013; Henry et al., 2016). In the subpolar North Atlantic, the sub-surface circulation is currently dominated at present by the northeastward flow of the North Atlantic Current (NAC), transporting warm and salty waters which become denser in the Nordic Seas, sink and flow back into the North Atlantic as deep overflow waters (see Daniault et al., 2016 and references therein). Any modification in the formation and intensity of the deep waters affects the AMOC with a strong impact on the northern hemisphere climate (e.g. Caesar et al., 2018, 2021). It is therefore critical to understand well the mechanisms leading to changes in the deep ocean intensity under various external (e.g. Earth's orbital variability) or internal (e.g. atmospheric CO_2 concentration, ice volume) climate forcings.

The sensitivity of ISOW both to orbital changes (Ellison et al., 2006; Kissel et al., 2009, 2013; Thornalley et al., 2013) and to regional melting events such as the 8.2 ka event (Kissel et al., 2013), was demonstrated during the warm period of the Holocene, based on sedimentological proxies (grain-size and magnetic properties). During the last glacial period, based on the same proxies, the strength of overflow waters, in particular the Iceland-Scotland Overflow Water (ISOW), has been shown

* Corresponding author. Université Grenoble Alpes, CNRS, IRD, Grenoble INP, IGE, Grenoble, France.
E-mail address: nathan.stevenard@univ-grenoble-alpes.fr (N. Stevenard).

https://doi.org/10.1016/j.quascirev.2024.109011
Received 11 June 2024; Received in revised form 16 October 2024; Accepted 16 October 2024
Available online 4 November 2024

to fluctuate on millennial timescales, in phase with the so-called Dansgaard-Oeschger (D-O) events (Dansgaard et al., 1993). The ISOW was intense during Greenland interstadials and weak but not completely absent during Greenland stadials (Rasmussen et al., 1996; Moros et al., 1997; Kissel et al., 1999, 2008; Ballini et al., 2006; Dokken et al., 2013; Wary et al., 2017). In a contradictory way, the records of another AMOC strength proxy, the protactinium (^{231}Pa) *versus* thorium (^{230}Th) ratio, suggest a complete collapse of AMOC at the Bermuda Rise (in the deep western North Atlantic basin) during Heinrich events in response to large iceberg discharges (McManus et al., 2004; Böhm et al., 2015; Henry et al., 2016). These two conflicting interpretations have led many studies to consider only the ^{231}Pa/^{230}Th ratio from the single Bermuda Rise site as a "benchmark" of AMOC changes over the last glacial period, ignoring the evidence of a still active deep Atlantic circulation during the coldest glacial events obtained from multiple sites distributed along the overflow paths (Kissel et al., 1999, 2008; Howe et al., 2016; Keigwin and Swift, 2017).

For periods beyond the last glacial period, the North Atlantic deep circulation changes are mainly documented by the geochemistry of the water masses using the carbon isotopic composition (δ^{13}C) of epibenthic foraminifera as a water-mass ventilation proxy (e.g. Duplessy et al., 1988; Curry and Oppo, 2005). The high-resolution reconstructions obtained from nearby the mid-Atlantic ridge (IODP U1308; 3871 m depth; Fig. 1; Hodell et al., 2008) and the Iberian margin (IODP U1385; 2587 m depth; Fig. 1; Hodell et al., 2023) and covering the last million years, show a well-defined glacial-interglacial variability of the ventilation of deep North Atlantic water masses. While well-ventilated North Atlantic Deep Water (NADW) dominated during interglacials (*s.l.*), the increased contribution of Southern Sourced Water (SSW) is observed during glacial periods. Over the same period, Grützner and Higgins (2010) used the Potassium (K) and Titanium (Ti) elemental ratio to track the Ti-rich volcanic-derived sediments transported by ISOW over the last 1.1 Ma. They showed that ISOW transported more (less) basaltic-rich sediment during interglacial (glacial) periods in phase with well (more poorly) ventilated deep water masses in the North Atlantic. They suggest that the reduction of volcanic-derived sediment could be the result of a SSW invasion in the Iceland basin. They also demonstrate an enhanced millennial-scale variability of the K/Ti record during glacial periods after crossing threshold of ice-volume growth reflected by benthic δ^{18}O values of 4.15–4.65 ‰ VPDB (Grützner and Higgins, 2010).

In addition to the studies described above, changes in the strength of North Atlantic bottom currents have been investigated in more detail

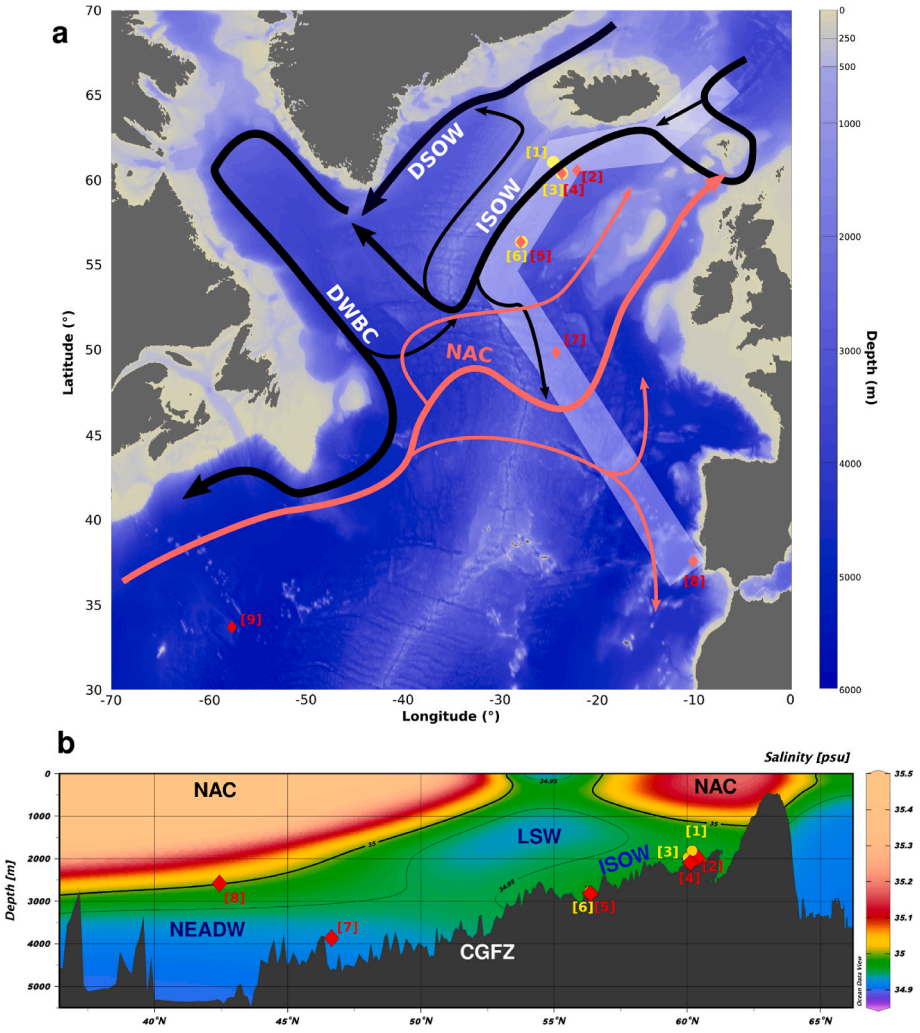

Fig. 1. Bathymetry and modern salinity section of the subpolar North Atlantic basin and location of the three pairs of cores studied here. A) Bathymetric map with the main deep (blue arrows) and sub-surface (dark pink) currents, the three pairs of cores (yellow circles) and other sites used in this study for discussions (red diamonds). B) Salinity section (as indicated in A by the shaded area) with the latitude and depth of each core represented on the map. [1] = MD03-2679-80Cq; [2] = core SU90-33; [3] MD03-2685-84Cq; [4] ODP site 983; [5] IODP site U1314; [6] MD03-2673-74Cq; [7] IODP site U1308; [8] IODP site U1385; [9] ODP site 1063. DSOW = Denmark Strait Overflow Water; ISOW = Iceland-Scotland Overflow Water; DWBC = . Deep Western Boundary Current; LSW = Labrador Sea Water; NAC = North Atlantic Current; NEADW = North East Atlantic Deep Water; CGFZ = Charlie-Gibbs Fracture Zone; NAC = North Atlantic Current.

during specific time intervals. Using stable carbon isotopes of benthic foraminifera and sortable silt mean grain-size ($\overline{SS}$) at a site located on the southern Gardar drift (IODP U1304; 3082 m water depth; Fig. 1), Hodell et al. (2009) suggested a weak circulation and poorly ventilated waters during the Termination II (T-II) and the first part of the last interglacial, with highest flow speed reached around 124 ka, in agreement with the establishment of well-ventilated deep-waters. Also based on benthic foraminifera $\delta^{13}C$, grain-size as well as ε_{Nd} from Bermuda Rise (ODP 1063; 4584 m water depth) and Gardar drift (ODP-983; 1983 m water depth) sites (Fig. 1), Deaney et al. (2017) show that the increase in deep North Atlantic ventilation during T-II was followed by an increase in bottom current intensity. On older timescales, Kleiven et al. (2011) produced $\overline{SS}$ and benthic foraminifera $\delta^{13}C$ records from MIS 18 to 22 at site ODP-983. They showed the continuous presence of well-ventilated water masses at ODP site 983, both during glacial and interglacial periods, with a strong orbital influence and abrupt increases of ISOW intensity during deglaciations. Therefore, these results, most of the time only focused on a short time interval and/or on a single site, lead to different interpretations of the mechanisms controlling past overflow intensity.

Additional and robust data would then help understanding in greater detail the mechanisms controlling orbital and suborbital changes in the intensity of overflow waters. The last four glacial-interglacial cycles (~400 ka) display the largest changes in Earth's insolation, atmospheric greenhouse gas concentrations, temperature and sea-level of the last million years (Tzedakis et al., 2009; Past Interglacials Working Group of PAGES, 2016). They therefore constitute a favorable period to study mechanisms and feedbacks of the deep North Atlantic circulation and its interactions with other components of the climate system (e.g. ice-sheet, sea-ice, atmosphere). However, some assumptions about the collapse (or not) of the deep Atlantic circulation during extremely cold events must be clarified before being able to examine the mechanisms of deep circulation intensity variability.

In this study, we use a multi-proxy approach on three sites from the subpolar North Atlantic, in order to evaluate the significance of "classical" ISOW intensity proxies used in this area, to document the glacial-interglacial changes in ISOW intensity over the last 400 ka, and to compare this new dataset with the current knowledge on the deep North Atlantic circulation over this period of time.

2. Regional settings and sedimentary material

At present, the thermohaline circulation in the North Atlantic consists of the warm and salty surface and intermediate (0–~1.5 km; Daniault et al., 2016) waters flowing northeastward across the North Atlantic basin, from the Gulf of Mexico to the Nordic Seas (Fig. 1). These waters cool and sink in the Nordic Seas convection areas during winter brine formation and then return southwestward into the deep Atlantic basin, passing over the Greenland-Scotland basaltic sills (Aagaard et al., 1985; Aagaard and Carmack, 1989; Mauritzen, 1996; Eldevik et al., 2009). Two return pathways are distinguished with two overflow water masses: the Denmark-Strait Overflow Water (DSOW) over the Greenland-Iceland sill and the ISOW over the Iceland-Scotland sill (Dickson and Brown, 1994; Saunders, 1994; Hansen and Østerhus, 2000; Østerhus et al., 2008; Daniault et al., 2016). These two deep currents form the modern lower limb of the North Atlantic Deep Water (NADW), a major component of AMOC.

The three sites we investigate in this study were collected during the P.I.C.A.S.S.O. (MD132/IMAGES XI) cruise onboard the R.V. *Marion Dufresne* in 2003 (Laj, 2003). At each site, a giant piston (Calypso) core was taken together with a CASQ core (labeled Cq) which better preserves the upper meters of sediment. These three pairs of Calypso and CASQ sediment cores are located on the pathway of the modern ISOW, along the eastern flank of Reykjanes Ridge between 1800 and 2800 m depth (Fig. 1). The two northernmost and shallowest pairs of cores were collected on the Björn and Gardar drifts, which are both characterized by fine contouritic facies formed by the persistent influence of ISOW flow (McCave et al., 1980; Bianchi and McCave, 2000). The southernmost and deepest pair of cores was taken further south on the Gardar drift (Fig. 1).

Core MD03-2679 was collected from the Björn drift (Fig. 1; 61°03.40′N; 24°32.42′W; 1812 m depth; 35.37 m long) and is characterized by olive-green, bioturbated and sometimes laminated clayey-silts. A few sandy layers visible at ~28.7, ~34.4 and ~34.7 m may be associated with tephra or turbidites. The CASQ core MD03-2680Cq taken at the same location is 10.96 m long and covers the upper 15.11 m of the Calypso core MD03-2679 (Fig. S1).

The second core, MD03-2685, is located on the Gardar drift (60°24.08′N; 23°38.39′W; 1977 m depth; 44.61 m long) (Fig. 1), close to the ODP site 983 (Fig. 1). This core is composed of homogeneous grayish to greenish clayey-silt to silty-clay. The sediment is sometimes bioturbated with isolated sand to gravel-sized clasts. It is coupled for its upper 17.2 m with the 11.3 m long CASQ core MD03-2684Cq (Fig. S1).

Core MD03-2673 is located farther south on the Gardar drift (Fig. 1; 56°21.91′N; 27°48.86′W; 2786 m depth; 39.05 m long). It is made of grey to brown silty-clays, frequently bioturbated with isolated sand to gravel-sized clasts that could be Ice-Rafted Detritus (IRD). Two diatom-rich layers are present at ~21.5 and ~36 m depth. Its upper 18 m are covered by the 11.85 m long CASQ core MD03-2674Cq (Fig. S1).

To compare the new records obtained from these three sites to ice-sheet volume and deep ocean ventilation changes, we selected two IODP cores for which high-resolution benthic foraminifera $\delta^{18}O$ and $\delta^{13}C$ records are available. These isotopic data are from the IODP site U1308 (Hodell et al., 2008) located east of the mid-Atlantic ridge (Fig. 1; 49°52.40′N; 24°14.17′W; 3871 m depth) and the IODP site U1385 (Hodell et al., 2023) located on the Iberian margin (Fig. 1; 37°34.17′N; 10°07.34′W; 2587 m depth). Both sites are bathed by the modern North East Atlantic Deep Water (NEADW).

3. Methods

We used a multi-proxy approach on the three studied cores, including high resolution (every one to two cm) measurements of elemental (X-Ray Fluorescence, XRF) and magnetic properties. In addition, we analyzed the grain-size of cores MD03-2673 and MD03-2679 at a lower resolution (every four to five cm), with a focus on MIS 7 and 9 (Stevenard et al., 2023).

3.1. Magnetic properties

For the analysis of magnetic properties, we have sampled all studied cores using u-channels taken in the center of the working half core for each section (Weeks et al., 1993). All magnetic properties were analyzed following the laboratory procedure described in detail in the Supplemental Material. The natural (NRM), anhysteretic (ARM) and isothermal (IRM) remanent magnetizations were measured on u-channels using 755R DC-SQUIDS cryogenic magnetometers from 2G Enterprise, placed within the μ-metal shielded room of the LSCE (Laboratoire des Sciences du Climat et de l'Environnement, Gif sur Yvette, France). The measurements were made every 2 cm with a pick-up coil resolution of 5.8 cm. The volume low field magnetic susceptibility (κ_{lf}) was also measured on u-channels every 2 cm with the same spatial resolution as for the remanent magnetization.

3.2. Grain-size analyses

For grain-size data analyses of cores MD03-2673 and MD03-2679, 2 cm^3 of sediment were taken from u-channels every 4–5 cm on MIS 7 and 9. This represents a total of 318 samples for core MD03-2673 and 265 samples for core MD03-2679. Grain size data were obtained from the detrital part of the sediment after removal of all biogenic content

(Supplemental Material) using the laser diffractometers Malvern Mastersizer 3000 and 2000 at LPG-BIAF (University of Angers, France) and GEOPS (University of Paris-Saclay, France) for cores MD03-2673 and MD03-2679, respectively. Grain-size distributions were corrected from IRD influence with the method developed by Stevenard et al. (2023) using End-Member Analyses (EMA) with the AnalySize GUI Matlab (Paterson and Heslop, 2015). The mean size of "sortable silt" ($\overline{SS}$) (mean size of the non-cohesive silt in the 10–63 μm range) was calculated following McCave and Andrews (2019) taking into account the IRD-corrected grain-size distributions to produce $\overline{SS}_{\text{IRD\_free}}$, a proxy of deep current intensity (Stevenard et al., 2023). In addition, the geometric mean grain-size ($\overline{X}_{\text{IRD\_free}}$) was calculated on the basis of the IRD corrected grain-size distribution, in order to also consider the grain-size variability of the finer grain-size fraction.

3.3. X-Ray Fluorescence measurements

The elemental composition of cores MD03-2673, MD03-2685 and MD03-2679 was analyzed using the 4th generation Avaatech core scanner available at the LSCE, on the "archive" half section of each core, with a 1 cm resolution and downcore and cross-core slits of 1.0 and 1.2 cm, respectively (Stevenard et al., 2023; details in Supplemental Material). To remove specimen effects (e.g. water content, matrix effect, burrows) which can impact the absorption of X-rays (Weltje and Tjallingii, 2008), we applied a Multivariate Log-ratio Calibration (Weltje et al., 2015). For this purpose, we analyzed 96, 85 and 90 discrete samples for cores MD03-2679, MD03-2673 and MD03-2685, respectively. These samples were selected (see details in Supplemental Material), and measured with the PANalytical Epsilon 3^{XLE} Energy Dispersive XRF spectrometer available at the LSCE. The Multivariate Log-Ratio Calibration of the three cores were realized using the GUI Matlab *Xelerate* (Weltje et al., 2015). As suggested by many studies, most of XRF data are expressed in log-ratios in this study (Aitchison, 1990; Weltje and Tjallingii, 2008; Weltje et al., 2015).

3.4. Age models

The chronologies of the three studied pairs of cores are produced in five steps (Figs. S1, S4-5). As a first step (1), we convert the CASQ depth scales to their respective Calypso depths. These conversions were done by aligning the ln(Ca/Ti) variations of the Calypso (from this study) and the CASQ (from T. Richter, personal communication) cores and the κ_{lf} for the deepest part of the CASQ cores, where no XRF data were available (Fig. S1). All alignments were made using the *AnalySeries* software (Paillard et al., 1996).

For the second step (2), we used Accelerator Mass Spectrometry (AMS) radiocarbon dates obtained on the planktic foraminifera species *G. bulloides* and *N. pachyderma* from the CASQ cores MD03-2680Cq and MD03-2674Cq. The 4 dates previously reported by Kissel et al. (2009) for these two cores are completed by unpublished dates obtained at the same time, as well as 5 new radiocarbon dates (Table 1), all obtained on the same two foraminifera species. All dates were converted into calendar age before present (BP) using the Marine20 calibration curve (Heaton et al., 2020), with a $\Delta R = 0$. The CASQs depths of the dated horizons were transferred to the Calypso depths. The radiocarbon dates cover the last 36 ka in core MD03-2680Cq and the last 10 ka in core MD03-2674Cq (Table 1). The age model of cores MD03-2679-80Cq was therefore constructed by linear interpolation between calibrated radiocarbon dates. It is constrained for core MD03-2673-74Cq both by radiocarbon dates for the last 10 ka, and below, down to 36 ka, by the alignment of ln(Ca/Fe) and κ_{lf} variations of this core to those of cores MD03-2679-80Cq. The age model of the last 36 ka of cores MD03-2685-84Cq is only based on the alignment with cores MD03-2679-80Cq using ln(Ca/Fe) and κ_{lf} variations.

As a third step (3), beyond 36 ka, we used the intensity of the Earth's magnetic field to correlate the three pairs of cores. Indeed, the prerequisites for a reliable sedimentary recording of the geomagnetic field changes (uniform magnetic mineralogy and grain-sizes) are fulfilled in the three pairs of cores (see **section 4.1.** and Figs. S2–S3). Thus, we used the ratio NRM/ARM as the record of relative paleointensity (RPI, Fig. S2). The Laschamp excursion dated at 41.1 ± 0.35 ka (Lascu et al., 2016) is clearly identified by marked lows in the RPI records. It was used as the first tie-point for this period in all three pairs of cores.

The fourth step (4) concerns the chronology of the pair of cores MD03-2685-84Cq, beyond 41 ka. We aligned the RPI and κ_{lf} variations of these cores to those of ODP-983 (Channell et al., 1997, 2013), in turn reported on the so-called "ice-core" chronology established by (Barker et al., 2015). This chronology is based on the alignment of oceanic surface changes (IRD counts, *N. pachyderma*%, coarse fraction%) to the millennial-scale variability of the Greenland synthetic temperature curve $GL_{T_}$syn (Barker et al., 2011) reported on AICC2012 ice core chronology (Bazin et al., 2013; Veres et al., 2013). This allowed us to transfer the AICC2012 chronology to cores MD03-2685-84Cq. We produced a Bayesian age model using the "*Undatable*" GUI Matlab software (Lougheed and Obrochta, 2019) including a constant age uncertainty of 1000 years for tie-points older than 41 ka. The resulting age model of core MD03-2685-84Cq is thus based on the transfer of radiocarbon dates from cores MD03-2679-80Cq (0–36 ka), the Laschamp excursion as a first tie-point around 41 ka, and the transfer of the Barker et al. (2015) chronology from ODP site 983 (>41–405 ka).

Table 1
AMS radiocarbon dates of cores MD03-2679-80Q and MD03-2673-74Q.

Lab code	Core	Depth CASQ (cm)	Depth Calypso (cm)	Material	14C age BP	Error	Age cal BP Marine20	2 σ	1 σ
Poz-10855	MD03-2679-80Q	0	60	*G. bulloides*	760[a]	30	215	331	152
Poz-10775	MD03-2679-80Q	83	243	*G. bulloides*	4860[b]	35	4943	379	194
Poz-10857	MD03-2679-80Q	171	441	*G. bulloides*	7800[a]	40	8081	311	151
SacA-68752	MD03-2679-80Q	215	528	*G. bulloides*	12855	40	14477	604	335
Poz-10858	MD03-2679-80Q	247	580	*G. bulloides*	17100[b]	90	19737	628	318
SacA-68753	MD03-2679-80Q	373	746	*N. pachyderma* sinistral	24430	110	27717	608	262
SacA-68754	MD03-2679-80Q	439	825	*N. pachyderma* sinistral	29010	180	30460	1165	656
SacA-68755	MD03-2679-80Q	502	899	*N. pachyderma* sinistral	32070	260	35691	1059	557
SacA-68756	MD03-2679-80Q	530	929	*G. bulloides*	32870	280	36523	1288	625
Poz-10769	MD03-2673-74Q	0	3	*G. bulloides*	1120[a]	30	548	215	112
Poz-10770	MD03-2673-74Q	122	304	*G. bulloides*	3910[b]	40	3713	360	183
Poz-10849	MD03-2673-74Q	146	359	*G. bulloides*	5690[b]	60	5890	422	207
Poz-10771	MD03-2673-74Q	202	566	*G. bulloides*	7520[b]	40	7797	292	158
Poz-10773	MD03-2673-74Q	345	790	*G. bulloides*	9440[a]	50	10112	389	188

The dates labeled Poz-# and SacA-# were obtained at the Poznan Radiocarbon Laboratory in Poland and at the national French accelerator ARTEMIS (UMS 2572, LMC14).

[a] Data from Kissel et al. (2009).

[b] Unpublished data.

As a fifth step (5), we used this newly produced MD03-2685-84Cq chronology as the reference for the two other pairs of cores. We transferred it to cores MD03-2679-80Cq and MD03-2673-74Cq by aligning their variations in RPI, κ_{lf} and ln(Ca/Fe) with those of core MD03-2685. Finally, we applied, for each pair of cores, Bayesian age models with "*Undatable*" (Lougheed and Obrochta, 2019), including radiocarbon dates, Laschamp excursion and age-depth tie points with the same 1000-year age uncertainties.

As a result, the sedimentation rates vary between 5 and 25 cm.ka^{-1}, with higher sediment accumulation during interglacial periods (Supplemental Material, Fig. S6). They reach 15–20 cm.ka^{-1} for warm periods and drop to between 5 and 10 cm.ka^{-1} during glacial periods. Therefore, the temporal resolution of high-resolution (1 cm) elemental records varies between 50 and 70 to 100–200 years. The temporal resolution of grain-size analysis (every 4–5 cm) varies between 200-350 and 400–1000 years.

To increase the quality of the comparison of our new data to previously published benthic δ^{13}C data, we revised the 0 to 400 ka age models of IODP sites U1385 (Hodell et al., 2023) and U1308 (Hodell et al., 2008). As the planktic δ^{18}O record from site U1385 is highly anti-correlated to Iberian margin sea surface temperatures (SST; Martrat et al., 2007), it is considered as a proxy of SST changes in North Atlantic. In this area, large-scale SST variations are synchronous with Greenland surface air-temperature changes recorded in ice cores (Davtian and Bard, 2023) and the correlation between the two records is commonly used to define age models (Hodell et al., 2015; 2023). Therefore, we aligned the variations of the planktic foraminifera (*G. bulloides*) δ^{18}O record of U1385 (Hodell et al., 2023) to GL$_T$_syn on the AICC2012 chronology (Barker et al., 2011). Once this age model of U1385 was produced, we aligned the variations of benthic foraminifera (*C. wuellerstorfi* and *C. kullenbergi*) δ^{18}O from U1308 (Hodell et al., 2008) to those from U1385 with our revised age-model (Figs. S8 and S9). Downcore benthic δ^{13}C changes are compared to cross-check the revised age model of site U1308 (Fig. S9).

We have then produced coherent age-models for our three studied P.I.C.A.S.S.O. pairs of cores (Fig. S7) and for the two IODP sites in North Atlantic (see Supplemental Material), all based on AICC2012 ice core chronology (Bazin et al., 2013; Veres et al., 2013).

4. Results

4.1. Magnetic mineralogy

Uniform magnetic mineralogy and magnetic grain-size are part of the prerequisites for the sediment to be a reliable recorder of the Earth's magnetic field. The characteristic remanent magnetization (ChRM) calculated after stepwise demagnetization of NRM indicates that the mean inclination obtained in each core is the one expected at these latitudes on the basis of a Geocentric Axial Dipole (GAD; Figs. S2 and S3) (MD03-2679 = 73.8° ± 8.6°, GAD = 74.5°; MD03-2673 = 67.6° ± 7.0°, GAD = 71.6°; MD03-2685 = 69.5° ± 8.3°, GAD = 74.1°). In addition, the three normalizations of NRM by κ_{lf}, ARM and IRM which account for the variations in magnetic concentration, yield similar changes indicating that all three ratios illustrate the variations in RPI (Fig. S2). We therefore considered the NRM/ARM ratio to construct the age model (see **section 3.4**).

S-ratio values ranging between 0.9 and 1 (with a mean of 0.95 for the three cores) indicate that the magnetic fraction is dominated by low coercivity minerals. The thermomagnetic curves (Fig. S10) confirm that this low coercivity mineral is magnetite, as already established on the Gardar Drift for the Holocene (Kissel et al., 2009) and the last glacial period (Kissel et al., 1999). The diagrams plotting ARM versus IRM (Fig. 2a–c) indicate significant changes in concentration, with smaller ones in magnetite grain size.

4.2. Downcore variability of magnetic concentration and grain-size

In this study, the tracers used to track the magnetic concentration changes, related to particles from the Iceland-Scotland basaltic province, are the κ_{lf} (corrected for the dilution by biogenic carbonates; see Supplemental Material) and the ARM (Kissel et al., 1999, 2008, 2009, 2013; Ballini et al., 2006). The magnetic grain-size changes are small but meaningful and we use the ARM/IRM ratio to illustrate them. The suggestion that magnetite grains are in aggregates and that their size is not a reliable proxy for bottom current strength (McCave, 2007) has been contradicted several times, in particular by Kissel et al. (2009). These authors showed, also on Gardar Drift sediments, that similar magnetic properties are obtained from the bulk sediments and on the magnetic fraction extracted without the use of ultrasounds, indicating that magnetites are interstitial within the sediment. The experiment has been repeated here and the same conclusion was reached that magnetites behave as free particles.

The magnetic concentrations and grain-sizes of the two northern sites MD03-2685-84Cq and MD03-2679-80Cq exhibit very similar range of values (Fig. 3) although discrete peaks observed in both magnetic concentration and grain-size in the MD03-2679-80Cq are not recorded in the cores MD03-2685-84Cq. In contrast, the magnetic concentration and grain-size in cores MD03-2673-74Cq are lower than in the two northern pairs of cores (Fig. 3).

Nevertheless, each of the three magnetic proxies exhibit the same type of variability in all three pairs of cores, and vary in phase, both on glacial-interglacial and millennial timescales (Fig. 3). The only exceptions concern two horizons in core MD03-2673-74Cq, which correspond to diatom ooze layers at terminations T-II and T-IV. High ARM/IRM values at these horizons most likely result from fine magnetic particles trapped in diatom shells. These two events obviously do not reflect

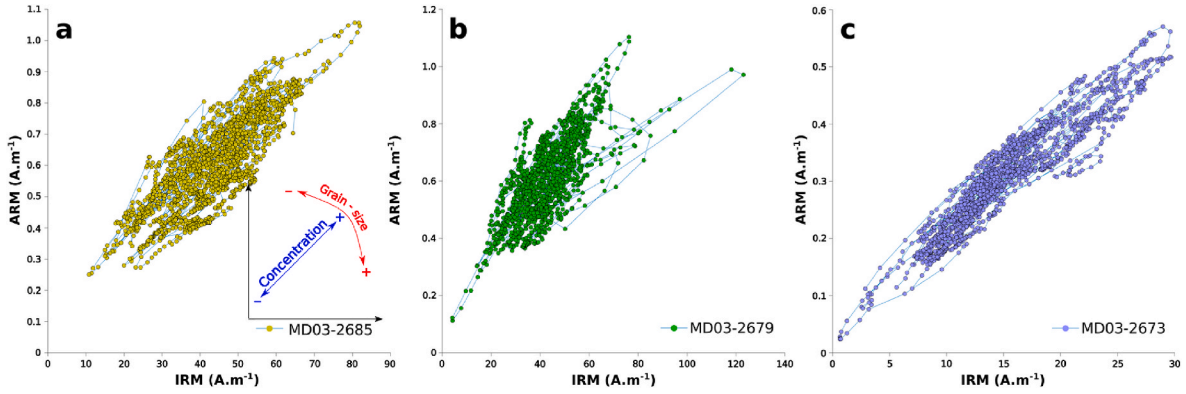

Fig. 2. ARM versus IRM plots of the three studied pairs of cores. ARM versus IRM plots showing magnetic concentration and grain-size dispersion of cores (a) MD03-2685-84Cq, (b) MD03-2679-80Cq and (c) MD03-2673-74Cq.

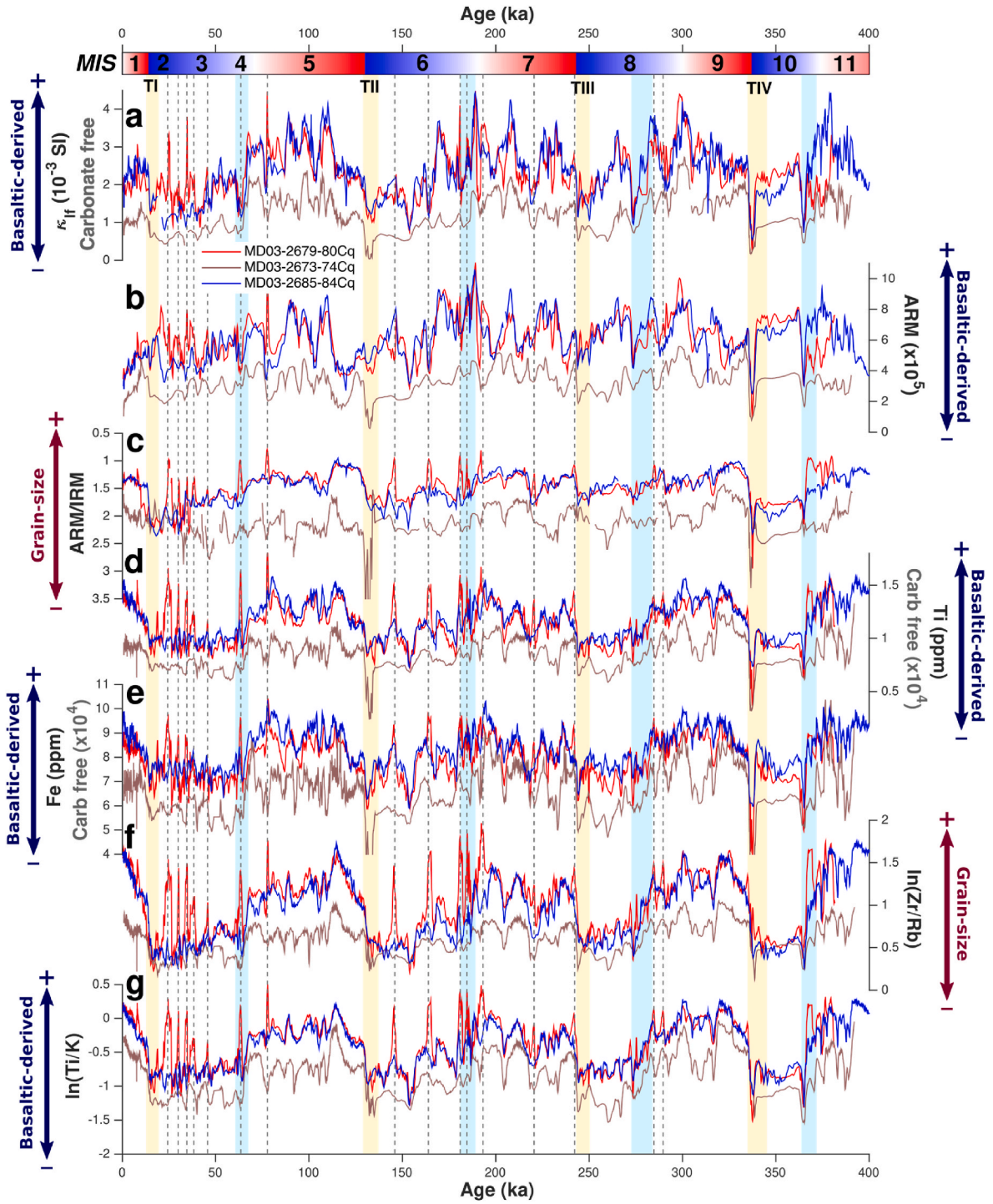

Fig. 3. Downcore magnetic and elemental proxy variability of the three pairs of cores over the last 400 ka. (a) The low field volume magnetic susceptibility corrected for biogenic carbonates, (b) the anhysteretic remanent magnetization (ARM), (c) the grain-size proxy ARM/IRM (coarser to lower values), (d) the Ti content (ppm) corrected for biogenic carbonates, (e) The Fe content (ppm) corrected for biogenic carbonates, (f) the grain-size ratio ln(Zr/Rb) and (g) the source ratio ln(Ti/K). Red = MD03-2679-80Cq; blue = MD03-2685-84Cq; brown = MD03-2673-74Cq. Red = MD03-2679-80Cq; blue = MD03-2685-84Cq; brown = MD03-2673-74Cq. The MIS boundaries are defined after Lisiecki and Raymo (2005) and the light yellow and blue vertical bars indicate respectively the terminations and glacial inceptions. Vertical dashed lines indicate peaks only detected in cores MD03-2679-80Cq.

hydrodynamical changes. In parallel, a clear glacial-interglacial variability is visible at the three sites, with higher magnetic concentration and coarser magnetic grain-size during interglacials (*s.l*) compared to glacial periods (Fig. 3). In addition, both interglacial and glacial periods are marked by millennial-scale variability of magnetic grain-size and concentration changes (Fig. 3). A fast increase in magnetic concentration and grain-size, marking the transition between glacial and interglacial deep North Atlantic circulation patterns, is observed at the end of each deglaciation (Fig. 3). The transitions from interglacial to glacial periods at 70, 190, 280 and 367 ka are marked by strong decreases in magnetic grain-size and concentration (Fig. 3a–c).

4.3. Downcore variability of elemental tracers

The elemental tracers used in this study to track the concentration related to basaltic-derived grains from the Iceland-Scotland basaltic province are the titanium (Ti) and iron (Fe) concentrations, which have been corrected for the dilution by biogenic carbonates (see Supplemental Material), as well as the ln(Ti/K) ratio, already used for the same purpose by Ballini et al. (2006) and Grützner and Higgins (2010). In contrast, the Zirconium (Zr) versus Rubidium (Rb) ratio is interpreted as a sedimentary grain-size proxy (Toyos et al., 2020; Wu et al., 2020; Toucanne et al., 2021; Stevenard et al., 2023; Lamy et al., 2024).

As already observed for magnetic tracers, all elemental proxies from the northern cores MD03-2679-80Cq and MD03-2685-84Cq show the same range of basaltic-derived grain concentration and grain-size values over the last 400 ka (Fig. 3). Some peaks detected in all elemental tracers in cores MD03-2679-80Cq are not visible in MD03-2685-84Cq records (Fig. 3, discussed in **section 5.1**), and they are in phase with the magnetic peaks described above. The Fe and Ti concentrations of basaltic-derived sediments exhibit systematically lower values in the southern cores MD03-2673-74Cq than in the two other northern pairs of cores (Fig. 3). The detrital grains are also finer in cores MD03-2673-74Cq than in the two northern sites during interglacial periods. These grain-size differences (ln(Zr/Rb) ratios) between the northern and southern sites are reduced or negligible during glacial periods (MIS 2, 6 or 10; Fig. 3). Compared to the other elemental proxies, this ratio is the only one showing this dampened North to South gradient. This point is discussed in **section 5.1**.

Elemental concentration and grain-size proxies vary in phase in the three sites (Fig. 3). This variability is defined by strong glacial-interglacial changes, with higher basaltic-derived grain concentration and grain-size during interglacials (*s.l.*) compared to during glacial periods (Fig. 3). Both periods are also marked by millennial scale events, in grain-size and basaltic-derived grain concentration (Fig. 3). The transitions between our glacial and interglacial conditions are marked by a strong increase of both concentration and grain-size, at the end of each deglaciation (Fig. 3). Transitions between interglacial and glacial values occur at 69, 191, 280 and 367 ka and are less abrupt than for deglaciations (Fig. 3). These transitions are sometimes punctuated by millennial scale events as observed during the MIS 7 to MIS 6 boundary (Fig. 3).

4.4. Downcore variability of the sortable fraction

The mean sortable silt free of IRD influence has been obtained from cores MD03-2679 and MD03-2673, with a focus on MIS 7 and MIS 9 (Stevenard et al., 2023).

Detrital grains are always finer in core MD03-2673 than in core MD03-2679 (Fig. 4). The glacial-interglacial variability is also well defined in the two cores, with finer grains during MIS 10, 8 and 6, and coarser ones during interglacials (*s.l.*). However, core MD03-2679 exhibits some peaks of coarser grain-size (as also recorded by magnetic and elemental proxies) that are not recorded in the other cores. These peaks tend to visually dampen the long-term variability in MD03-2679 grain-size records, even though glacial-interglacial changes remain present throughout the core. The records show strong decreases at around 200, 225, 280 and 295 ka, almost reaching the full glacial grain-size values (Fig. 4). The transitions between glacial to interglacial occur at the end of deglaciations, with sharp and strong increases in grain-size (Fig. 4).

5. Discussion

5.1. Robust tracers of the strength of the southward flowing ISOW

The robustness of a multi-proxy approach to track past ISOW intensity in this area was demonstrated by Ballini et al. (2006) over the last glacial period. Most of the proxies used in this study indicate a high coefficient of correlation between them (Table 2), except for the $\overline{SS}$ and

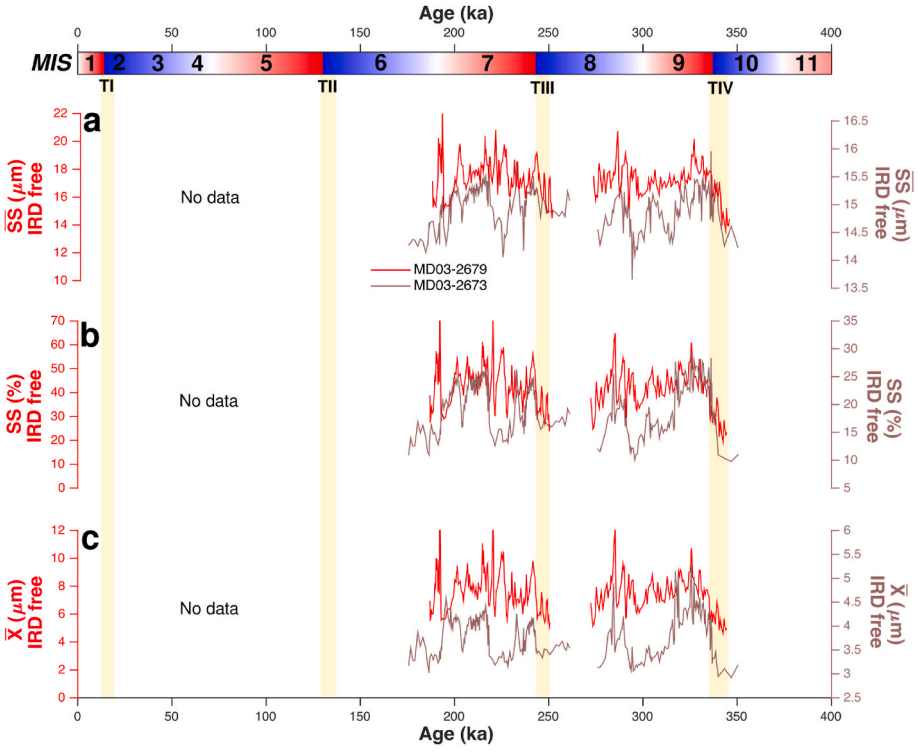

Fig. 4. Downcore grain-size proxy variability of the cores MD03–2679 and MD03–2673 during MIS 7 and 9. (a) The mean-size of sortable silt fraction (μm), (b) the percentage of sortable silt fraction and (c) the mean grain-size. The three tracers were calculated from the IRD-corrected grain-size distributions from Stevenard et al. (2023). Red = MD03-2679; brown = MD03-2673. The MIS boundaries are defined after Lisiecki and Raymo (2005) and the light yellow vertical bars indicate the terminations. Note that the y-scales on the right for core MD03-2673 and on the left for core MD03-2679.

ARM that show significant differences with the other tracers. As the sediment is composed by more abundant fine particles (<10 μm) than coarse ones (>10 μm), the correlation coefficient between ARM/IRM and ln(Zr/Rb) is higher with the mean grain-size than with $\overline{SS}$. This result also confirms that the magnetic grain-size varies in the micrometric range as demonstrated by Kissel et al. (2009) for the Holocene. The high correlation coefficients between most grain-size and concentration proxies suggest that they all well record the variability of ISOW strength. This result extends over the last 400 ka the robustness of the multi-proxy approach initially established for the Holocene (Kissel et al., 2009, 2013) and the last glacial period (Kissel et al., 1999, 2008; Ballini et al., 2006).

The most visible downcore differences between cores relate to the peaks observed in all magnetic, elemental and sortable silt records mainly during glacial or inception periods, at the site of cores MD03-2679-80Cq (Figs. 3 and 4). This pair of cores was collected from the Björn drift, closer to the Iceland slope than the two other sites located on the Gardar drift (Fig. 1). Due to its proximity to the Iceland ice-sheet during glacial times, this site may be affected by gravity flow processes associated with Iceland glacier's surges (Lacasse et al., 1998). As ISOW acts as a contour current East of the Reykjanes Ridge, it may transport this turbiditic material from Iceland downstream to the most proximal of our sites (MD03-2679-80Cq), locally increasing both magnetic and basaltic-derived grain concentration, as well as the detrital mean grain-size, over short periods of time. Therefore, the peaks recorded in cores MD03-2679-80Cq only may reflect changes in sedimentary processes off Iceland rather than in deep current intensity. On millennial timescales, small differences may be observed between the various proxies (Figs. 3 and 4) depending on local processes. However, glacial-interglacial changes are always visible, which suggests that the three sites, bathed by the same bottom current, are affected by the same environmental processes.

Previous studies demonstrated the presence of a North to South gradient of magnetic concentration and grain-size, deposited under the influence of the southward flow of ISOW, during the Holocene (Kissel et al., 2009, 2013; Thornalley et al., 2013) and the last glacial period (Kissel et al., 1999, 2008). All proxy records show very similar variations in both the southern site of cores MD03-2673-74Cq and the two northern sites, despite a systematically lower basaltic-derived grain concentration and finer grains in the southernmost cores (compared to the northern ones). Interestingly, this North to South gradient, expressed in the ARM/IRM ratio and physical grain-size proxies, is less important or absent in the ln(Zr/Rb) records during glacial periods (Fig. 3c & 4). The interpretation of ln(Zr/Rb) in terms of grain-size proxy is based on the fact that the Zr-rich grains are more mainly in the 8–62 μm fraction, while the Rb-rich grains are more represented by sediment finer than 8 μm (Wu et al., 2020). The mean detrital grain-size drastically decreases to 5–6 μm and 3 μm in cores MD03-2679-80Cq and MD03-2673-74Cq, respectively, during glacial periods (Fig. 4). Therefore, the observed glacial loss of North-South gradient in the ln(Zr/Rb) ratio may be linked to a decreased amount of "coarse" Zr-rich grains transported along the Reykjanes Ridge during glacial times, both North and South of the study area. In this context of low content of Zr-rich grains, the absolute values of ln(Zr/Rb) may be biased and so is the gradient between our northern and southern records. Therefore, these gradient differences in the ln (Zr/Rb) ratios during glacial periods are more related to the way this ratio records grain-size changes than to spatial changes in the deep current affecting the area. In any case, the ARM/IRM ratio and IRD-corrected mean grain-size, do not show this decrease of the North to South gradient. Nevertheless, the observation of a North to South gradient in all proxies used, except the glacial ln(Zr/Rb) for the reasons explained above, extends over the last 400 ka the observations of Kissel

Table 2
Matrices of correlation between the different proxies used in this study for each pair of cores. The upper right corner indicates the Pearson correlation, while the lower left corner indicates the p-value. Bold values represent correlations that are not statistically significant (p-value > 0.01).

MD03-2673-74Cq										
Fe		0.93	0.75	0.77	0.51	0.76	−0.62	***−0.05***	0.28	0.40
Ti	0.00		0.86	0.76	0.46	0.85	−0.70	***0.06***	0.35	0.43
ln(Ti/K)	0.00	0.00		0.61	0.23	0.96	−0.60	***0.14***	0.47	0.50
κ_{lf}	0.00	0.00	0.00		0.75	0.66	−0.47	***0.03***	0.26	0.28
ARM	0.00	0.00	0.00	0.00		0.26	−0.28	***−0.08***	***0.09***	***0.11***
ln(Zr/Rb)	0.00	0.00	0.00	0.00	0.00		−0.60	***0.09***	0.40	0.44
ARM/IRM	0.00	0.00	0.00	0.00	0.00	0.00		−0.30	−0.54	−0.59
SS (μm)	***0.33***	***0.25***	***0.01***	***0.62***	***0.16***	***0.12***	0.00		0.79	0.54
SS (%)	0.00	0.00	0.00	0.00	***0.11***	0.00	0.00	0.00		0.92
Mean (μm)	0.00	0.00	0.00	0.00	***0.06***	0.00	0.00	0.00	0.00	
MD03-2679-80Cq										
Fe		0.90	0.88	0.50	0.20	0.76	−0.67	0.30	0.47	0.45
Ti	0.00		0.96	0.43	0.05	0.89	−0.76	0.44	0.58	0.56
ln(Ti/K)	0.00	0.00		0.50	0.10	0.97	−0.79	0.46	0.60	0.56
κ_{lf}	0.00	0.00	0.00		0.76	0.45	−0.41	***0.02***	0.20	0.17
ARM	0.00	0.05	0.00	0.00		***0.00***	***0.02***	−0.18	***−0.04***	***−0.03***
ln(Zr/Rb)	0.00	0.00	0.00	0.00	***0.99***		−0.79	0.49	0.59	0.55
ARM/IRM	0.00	0.00	0.00	0.00	***0.47***	0.00		−0.59	−0.65	−0.61
SS (μm)	0.00	0.00	0.00	***0.75***	0.00	0.00	0.00		0.93	0.91
SS (%)	0.00	0.00	0.00	0.00	***0.55***	0.00	0.00	0.00		0.98
Mean (μm)	0.00	0.00	0.00	0.00	***0.62***	0.00	0.00	0.00	0.00	
MD03-2685-84Cq										
Fe		0.93	0.88	0.58	0.15	0.75	−0.60			
Ti	0.00		0.96	0.59	***0.05***	0.89	−0.71			
ln(Ti/K)	0.00	0.00		0.60	0.06	0.96	−0.80			
κ_{lf}	0.00	0.00	0.00		0.71	0.49	−0.49			
ARM	0.00	***0.03***	0.01	0.00		−0.16	***0.06***			
ln(Zr/Rb)	0.00	0.00	0.00	0.00	0.00		−0.80			
ARM/IRM	0.00	0.00	0.00	0.00	***0.01***	0.00				
SS (μm)										
SS (%)										
Mean (μm)										

et al. (1999, 2008, 2009, 2013) for the last 60 ka, indicating a southward flow with the basaltic sill as the major source of basaltic-derived sediment.

The final point of this section, based on the previous observations discussed above, is that the proxies used in this study can be used as robust tracers of the past intensity of a deep current, flowing southward and transporting basaltic-derived grains originating from a northern source (i.e. the sill), by a deep current flowing southward and bathing the three studied sites. By analogy to the present deep North Atlantic circulation, we associate this deep current to ISOW in the following sections.

5.2. Persistent influence of ISOW over the last 400 ka

In the previous section, we interpret the concentration and grain-size proxies as faithfully recorders of past changes in ISOW relative vigour. Previous works demonstrated a persistent influence of the deep subpolar North Atlantic circulation over the last glacial period (Kissel et al., 1999, 2008). Indeed, the pattern of variations in basaltic-derived material content from one site to another along the ISOW, DSOW and the Deep Western Boundary Current (DWBC; Fig. 1) pathways is the same during Greenland warm (interstadials) and cold (stadials) events, with lower values during the latter illustrating a damping rather than an off-mode of the bottom circulation dynamics. Our records over the last 400 ka also indicate a well-preserved North-South glacial gradient from northern sites to the southern site. This North-South gradient suggests that the circulation was not entirely turned off during glacial periods.

Magnetic data are affected by the smoothing effect of the pick-up coil resolution (5.8 cm) of the high-resolution magnetometers and of the susceptibility meter adapted for u-channels, particularly during glacial periods characterized by low sedimentation rates (5–10 cm.ka^{-1}; Fig. S6). Elemental data from XRF analyses, which have a centimetric resolution with no smoothing, indicate globally similar changes (although slightly more abrupt) compared to magnetic data, in particular during Heinrich events. No "off mode" is thus smoothed out of the magnetic data because of the pick-up coil resolution. This result is confirmed by high sedimentation rates cores from the subpolar North Atlantic, which indicate a reduced (but not absent) overflow during millennial-scale events of the last glacial period (Kissel et al., 1999, 2008). Moreover, the "glacial" carbonate-free κ_{lf} values of the two northern sites vary between 10 and 20.10^{-4} SI, in agreement with those obtained by (Kissel et al., 1999; Kissel, 2005) from core SU90-33 from the Iceland basin. The southern and deeper site also show κ_{lf} values (between 5 and 11.10^{-4} SI) in the range of a sedimentation controlled by ISOW during glacial periods (Kissel et al., 1999; Kissel, 2005). As a comparison, the κ_{lf} values in core SU90-08 located in the Ruddiman belt show κ_{lf} values does not exceeding 3.10^{-4} SI during glacial periods, besides the Heinrich peaks (Kissel, 2005). Corrected for the carbonate content, these values increase up to about 5.10^{-4} SI at the maximum, significantly weaker in the cores bathed by ISOW. Therefore, along the ISOW path, the signal is strongly reduced during glacial periods but still present along the Reykjanes Ridge between 1800 and 2800 water depth, suggesting a continuously active deep-water flow over the last 400 ka.

This new interpretation is not consistent with the common idea emerged for a few decades of an "off mode" of the AMOC occurring during Heinrich events or stadials. This hypothesis was first described by (Rahmstorf, 2002) and heavily supported by the ^{231}Pa/^{230}Th ratio records from Bermuda Rise (4500 m), considered for years as a reference data set of AMOC changes. However, recent studies showed that the AMOC collapse during HS1, as recorded by the ^{231}Pa/^{230}Th ratio at this Bermuda Rise site where the production ratio is attained (McManus et al., 2004), is not consistent with data from other North Atlantic sites, in particular from different water-depths (Gherardi et al., 2009; Bradtmiller et al., 2014; Ng et al., 2018; Süfke et al., 2019). More recently, using the intermediate complexity climate model Bern 3D, Pöppelmeier et al. (2023) showed that the ^{231}Pa/^{230}Th values of Bermuda Rise during HS1 can be reproduced with an AMOC reduction of 30% from the Last Glacial Maximum (LGM), without any collapse of the AMOC. Consequently, the "off mode" of the AMOC as suggested by the Bermuda Rise ^{231}Pa/^{230}Th records may simply reflect local spatial changes of one deepest branch of the NADW during the HS1 AMOC slowdown. The recent effort to understand the changes in the Bermuda Rise ^{231}Pa/^{230}Th records and our new data provide robust arguments to disprove a complete collapse of AMOC, during Heinrich events or any other periods, and reinforce the interpretation that over the last 400 ka, North Atlantic deep waters are continuously active with an intensity varying in time, depending on the climatic periods.

Another working hypothesis concerns the formation of Glacial North Atlantic Intermediate Water (GNAIW) South of Iceland, which would be formed during glacial times by a southward migration of the convection areas (Duplessy et al., 1988; Lynch-Stieglitz et al., 2007; Lynch-Stieglitz, 2017). This modified water mass is supposed to replace NADW and to flow at shallower depths during glacial periods. Again, the previous studies of Kissel et al. (1999, 2008) showed highly similar glacial millennial-scale changes in deep-current intensity records from sites located to the North and South of the Iceland-Scotland basaltic sill. This result implies that the same water mass actively passed over the sills, and therefore that the convection persistently occurred to the North of the sills during the last glacial period. More recently, Howe et al. (2016) on the basis of a εNd synthesis during the LGM, proposed the glacial presence of two water masses in the Atlantic basin. The first one is GNAIW, originating from a convection area South of Iceland and affecting the intermediate circulation. The second one is the Glacial North Atlantic Deep Water (GNADW), which corresponds to a slower NADW with a decreased influence towards the South. In-phase variations of our new records from intermediate (1800–2000 m) and deep (2800 m) sites over the last 400 ka suggest that the three sites are affected by the same water mass. The question remains to identify this water mass. In a scenario where only GNAIW (formed to the South of Iceland) affects our sites, Iceland would be the major contributor of basaltic sediments, mostly *via* gravity flow events (Lacasse et al., 1998; Sigmarsson et al., 2008). This fine turbiditic material would be winnowed downstream by bottom deep-currents as suspended load (Lacasse et al., 1998). In that case, the detrital mean grain-sizes would increase due to the proximity of the source compared to the Iceland-Scotland sill. However, all our grain-size proxies always exhibit finer grain-sizes during glacial periods compared to interglacials (*s.l*). The only exceptions concern the peaks detected in the pair of cores MD03-2679-80Cq, interpreted as turbiditic events delivering basaltic material resulting from "pulses" of Iceland's glaciers. These cores are the closest to the Iceland and show drastic increases in grain-size and basaltic-derived concentration in response to these specific events. Nevertheless, the systematic decrease in the mean grain-size during glacial periods compared to interglacials suggests that the Iceland-Scotland sill might be the major source of basaltic sediments throughout the last 400 ka. To verify this hypothesis, a record of bottom-current intensity from a location to the North of the sill would be needed. Unfortunately, such records in the Nordic Seas are not yet available over the last 400 ka. However, Kissel et al. (1999, 2008) showed that during the most recent glacial period (25–65 ka), their study sites recorded the same and in-phase deep-current intensity to the North and South of the sill. Therefore, we favor the interpretation that GNADW (here, ISOW) was formed in the Nordic Seas and persistently affected the deep subpolar North Atlantic basin with various intensities over the last 400 ka.

5.3. Glacial - interglacial variability of ISOW intensity

Glacial - interglacial changes in ISOW strength were previously studied by Grützner and Higgins (2010). The authors conclude that during interglacials, the amount of basaltic-derived sediments transported from the sill to the Iceland basin is higher than during glacial periods, where the sedimentation may be affected by another deep water

mass, as the "Lower Deep Water" from the southern hemisphere. Their hypothesis is mainly based on the benthic $\delta^{13}C$ record from IODP site U1308 (Hodell et al., 2008) that is located deeper and further South compared to their study site IODP U1314. The presence of SSW at the IODP site U1314 (which is also the same location as cores MD03-2673-74Cq) would therefore indicate that this site is affected by another water mass than the two northern sites, which are bathed by well-ventilated deep-water as indicated by the benthic $\delta^{13}C$ record from ODP site 983 (Raymo et al., 2004). However, our results show a North to South sediment flux and in phase variations between our three study sites, regardless of the water-depth and location, indicating that our three sites are bathed by the same water mass. Therefore, the hypothesis proposed by Grützner and Higgins (2010) seems to be incompatible with our results and we suggest that the deep southern Gardar drift down to 2800 m water-depth is only affected by ISOW over the last 400 ka.

Our results also show fast ISOW strength changes that occur during periods of fast ice-sheet growth or melt, as indicated by the benthic foraminifera $\delta^{18}O$ records from IODP sites U1385 and U1308 (Fig. 5; Hodell et al., 2008, 2023). This is consistent with the results from Grützner and Higgins (2010) and confirms the importance of ice-volume changes in the glacial - interglacial deep ocean circulation. Grützner and Higgins (2010), on the basis of only a single elemental ratio from a single

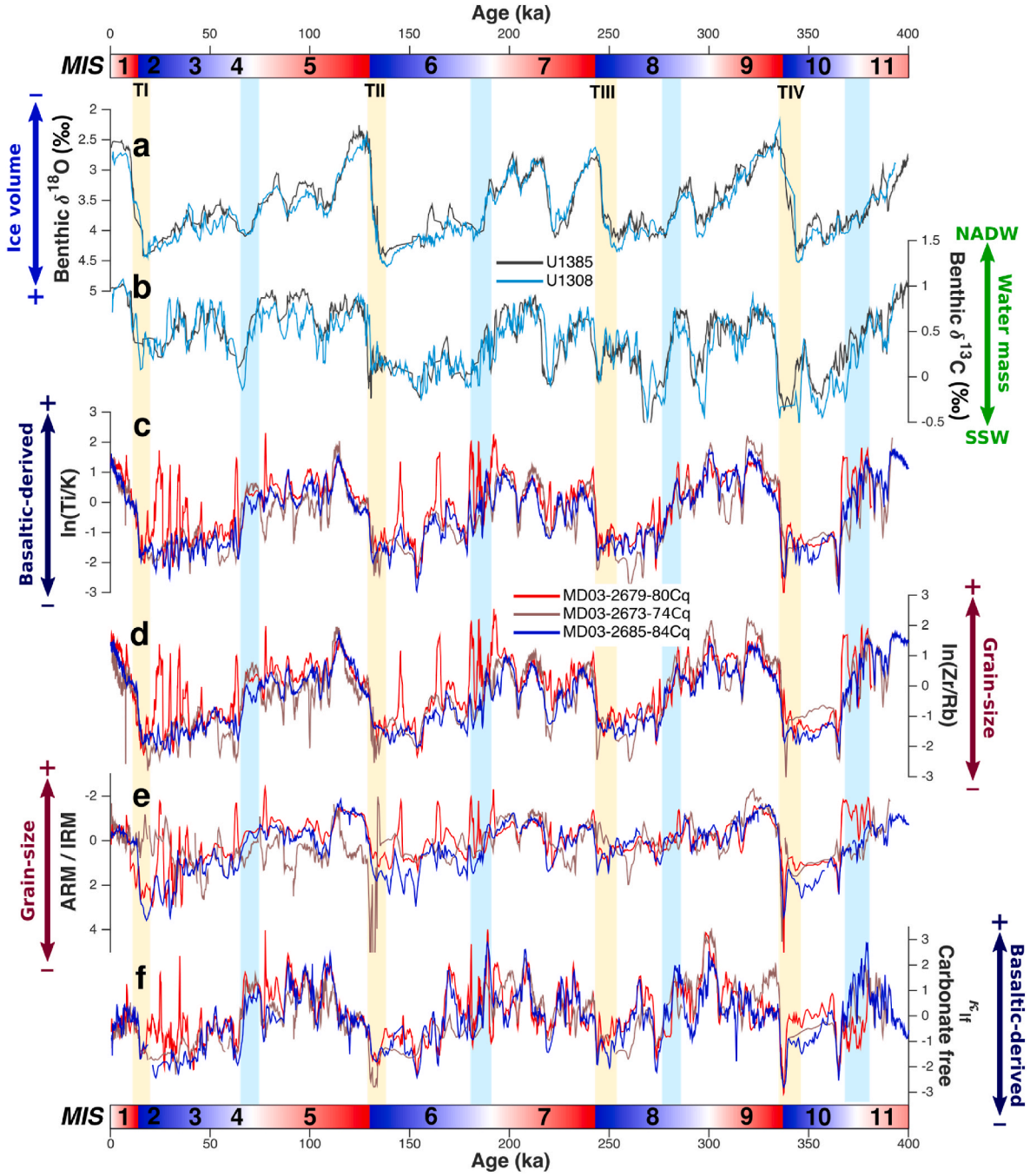

Fig. 5. Comparison of normalized ISOW intensity tracers (see Supplemental Material) with the ice-sheet volume and deep water mass ventilation proxies from the IODP sites U1308 (Hodell et al., 2008) and U1385 (Hodell et al., 2023). (a) Benthic $\delta^{18}O$, (b) benthic $\delta^{13}C$, (c) the normalized source ratio ln(Ti/K), (d) the normalized grain-size ratio ln(Zr/Rb), (e) the normalized magnetic grain-size ratio ARM/IRM and (f) the normalized volume low field magnetic susceptibility free of biogenic carbonate influence. MIS boundaries are defined after Lisiecki and Raymo (2005). Light-yellow vertical bars and blue vertical bars indicate terminations and transitions between interglacial to glacial ISOW states, respectively.

site, suggest a "threshold" in ice-volume which would enhance the millennial-scale variability of ISOW during glacial periods. Our data, based on a multi-proxy approach (with more sensitive XRF analytical measurements and calibration; see **section 3.3.**) and multi-sites, confirms this millennial-scale variability during glacial periods, but also shows its existence during interglacial periods (*s.l*).

We have compared our data of ISOW strength with deep-water ventilation from IODP sites U1308 (Hodell et al., 2008) and U1385 (Hodell et al., 2023, Fig. 1), all on the same chronological scale. Both sites exhibit a very similar pattern of deep ventilation changes, most of the time varying in phase with our sedimentary records of ISOW vigour (Fig. 5). When the ISOW strength is strong during interglacials (*s.l.*), the deep North Atlantic basin is well ventilated, and *vice versa* during glacial periods. The low sedimentation rates observed during glacial periods (Fig. S6) also suggest a reduced advective transport. Superimposed on these long-term changes, millennial-scale changes of ISOW vigour are accompanied by in-phase deep ventilation changes (Fig. 5). The more vigorous the ISOW, the better ventilated the deep North Atlantic. Three exceptions concern MIS 3, 8 and the end of MIS 10, where the ISOW is slow and the deep North Atlantic well-ventilated, whereas millennial-scale changes in deep-current intensity and deep-water ventilation remain in phase. This high degree of similarity between ISOW strength and deep-water ventilation changes suggests a closely link between overflow vigor and the southern extent of (G)NADW in the Atlantic basin over the last 400 ka. This relationship was already proposed by Kleiven et al. (2011) for older periods (MIS 18 to 22). We propose that overflows which form the lower limb of NADW may modulate the southern extent of this water mass into the Atlantic basin. When overflows are more vigorous, the volume of Northern Source Water (NSW) entering in the deep North Atlantic basin is more important and this water mass "pushes" further south or deeper the SSW. In a reverse scenario, when overflows slow down, the volume of NSW in the North Atlantic basin decreases and SSW passively invades the deep North Atlantic basin. In this proposed mechanism, SSW acts as a passive opportunistic component of the deep Atlantic circulation, by only being modulated by changes in the NSW vigor. The situation may be slightly different during the particular cases of MIS 3 and the end of MIS 8 and 10, where the deep-water masses are well ventilated and ISOW is weak, while millennial-scale variability is preserved. During these three specific periods, a low intensity of ISOW would lead to an increase of SSW influence in the deep North Atlantic basin. Two hypotheses could explain this situation. First, SSW may not be a passive component of ocean circulation and strengthens when NSW slows down (and *vice versa*), except during MIS 3 and the end of 8 and 10 where both water masses are slow for an unknown reason. The second hypothesis concerns the other components of NSW, such as DSOW or Labrador Deep Water (LDW), which could be more vigorous than ISOW during MIS 3, 8 and 10 and contribute more to a southward extent of NSW. However, records of the DSOW strength variability are conflicting, indicating a strong DSOW during interglacial (Mazaud et al., 2012) or glacial (J. Channell, 2006) periods depending on the core's water-depth. Therefore, the lack of robust, continuous and long-term deep vigour records of LSW, DSOW or SSW does not allow us to disentangle these hypotheses. More deep-water strength reconstructions would be needed to better understand the causal relationship between the vigour of the deep North Atlantic circulation and the deep-water ventilation.

6. Conclusion

We report here a reconstruction of the past ISOW strength over the last 400 ka using multi-proxy (magnetic, elemental and sortable silt) analysis of the detrital fraction of three sedimentary marine pairs of cores. The results highlight the following points.

- All our proxies, whatever their nature or meaning (elemental, magnetic and microgranulometry), consistently record the same variability of the past vigour of ISOW.
- The southernmost site is characterized by a lower basaltic-derived grain concentration and finer grain-size compared to the two northern sites, which show very similar variations and values for each proxy.
- Our results indicate a deep-current continuously flowing southward over the last 400 ka, suggesting no "off-mode" of AMOC in this area, always bathed by the (Glacial) North Atlantic Deep Water.
- The Iceland-Scotland basaltic sill acts as the major sediment supply during the last 400 ka, supporting the idea that convection areas in the Nordic Seas are always active.
- The ISOW strength is marked by a well-defined glacial - interglacial variability, superimposed by millennial-scale variability, during glacial and interglacial periods.
- The observed variations of ISOW vigour are in phase with deep-water ventilation changes further South in the North Atlantic basin on both orbital and millennial timescales.

Finally, our results bring new information about the deep circulation along the Gardar Drift, raise a number of questions and show that more data are needed with a good geographical distribution (e.g. along DSOW and to the North of the sills) to better decipher deep oceanic changes and mechanisms over the last 400 ka.

CRediT authorship contribution statement

N. Stevenard: performed grain-size, magnetic, XRF analysis, prepare radiocarbon samples, made the data processing, wrote the manuscript. **C. Kissel:** contributed to the development of the discussion, performed magnetic measurements on CASQ-cores, provided radiocarbon data and improved the manuscript. **A. Govin:** helped with XRF analysis, performed magnetic measurements, and contributed to improved the manuscript and. **C. Wandres:** helped with magnetic measurements and contributed to improved the manuscript.

Data availability

The U1308 and U1385 isotopic datasets are available in the Pangaea database (https://doi.org/10.1594/PANGAEA.762947 and https://doi.org/10.1594/PANGAEA.951401). The magnetic data from the ODP site 983 are available in the Pangaea database (https://doi.org/10.1594/PANGAEA.808979). Grain-size data of cores MD03-2673 and MD03-2679 are available in the Pangaea database (https://doi.org/10.1594/PANGAEA.950962 and https://doi.org/10.1594/PANGAEA.950966). The tie-points, magnetic and elemental (XRF) data sets are currently waiting for the publication in the Pangaea database.

Declaration of competing interest

The authors declare that they have no known competing financial interests or personal relationships that could have appeared to influence the work reported in this paper.

Acknowledgment

We are grateful to the chief scientist (C. Laj) and the crew of the R.V. *Marion Dufresne* for collecting the three sediment cores during the P.I.C.A.S.S.O. cruise. We thank A. Van Toer (LSCE) for technical support for the XRF and magnetic analyses. We are grateful to N. Vazquez-Riveiros, S. Toucanne and D. Swingedouw for fruitful discussions. N.S. acknowledges a PhD grant from the Commissariat à l'Energie Atomique et aux Energies Alternatives (CEA). A.G. acknowledges support from ANR (Grant ANR-18-BELM-0001-06). This work was supported by the CEA, the Centre National de la Recherche Scientifique (CNRS) and by the

French National program LEFE (Les Enveloppes Fluides et l'Environnement), under the project DECORATING (Dynamique des principaux courants profonds de l'Atlantique lors des périodes chaudes du passé: étude des interglaciaires des derniers 450 000 ans). We would like to thank the associate editor and the two anonymous reviewers for their comments and suggestions, which help us to improve the quality of our manuscript.

Appendix A. Supplementary data

Supplementary data to this article can be found online at https://doi.org/10.1016/j.quascirev.2024.109011.

Data availability

All new data are currently submitted to the PANGAEA database.

References

Aagaard, K., Carmack, E.C., 1989. The role of sea ice and other fresh water in the Arctic circulation. J. Geophys. Res. 94, 14485–14498. https://doi.org/10.1029/JC094iC10p14485.

Aagaard, K., Swift, J.H., Carmack, E.C., 1985. Thermohaline circulation in the arctic mediterranean seas. J. Geophys. Res. 90, 4833–4846. https://doi.org/10.1029/JC090iC03p04833.

Aitchison, J., 1990. Relative variation diagrams for describing patterns of compositional variability. Math. Geol. 22, 487–511. https://doi.org/10.1007/BF00890330.

Ballini, M., Kissel, C., Colin, C., Richter, T., 2006. Deep-water mass source and dynamic associated with rapid climatic variations during the last glacial stage in the North Atlantic: a multiproxy investigation of the detrital fraction of deep-sea sediments. G-cubed 7, 2005GC001070. https://doi.org/10.1029/2005GC001070.

Barker, S., Knorr, G., Edwards, R.L., Parrenin, F., Putnam, A.E., Skinner, L.C., Wolff, E., Ziegler, M., 2011. 000 years of abrupt climate variability. Science 334, 347–351. https://doi.org/10.1126/science.1203580, 800.

Barker, S., Chen, J., Gong, X., Jonkers, L., Knorr, G., Thornalley, D., 2015. Icebergs not the trigger for North Atlantic cold events. Nature 520, 333–336. https://doi.org/10.1038/nature14330.

Bazin, L., Landais, A., Lemieux-Dudon, B., Toyé Mahamadou Kele, H., Veres, D., Parrenin, F., Martinerie, P., Ritz, C., Capron, E., Lipenkov, V., Loutre, M.-F., Raynaud, D., Vinther, B., Svensson, A., Rasmussen, S.O., Severi, M., Blunier, T., Leuenberger, M., Fischer, H., Masson-Delmotte, V., Chappellaz, J., Wolff, E., 2013. An optimized multi-proxy, multi-site Antarctic ice and gas orbital chronology (AICC2012): 120–800 ka. Clim. Past 9, 1715–1731. https://doi.org/10.5194/cp-9-1715-2013.

Bianchi, G.G., McCave, I.N., 2000. Hydrography and sedimentation under the deep western boundary current on Björn and Gardar Drifts, Iceland Basin. Mar. Geol. 165, 137–169. https://doi.org/10.1016/S0025-3227(99)00139-5.

Böhm, E., Lippold, J., Gutjahr, M., Frank, M., Blaser, P., Antz, B., Fohlmeister, J., Frank, N., Andersen, M.B., Deininger, M., 2015. Strong and deep Atlantic meridional overturning circulation during the last glacial cycle. Nature 517, 73–76. https://doi.org/10.1038/nature14059.

Bradtmiller, L.I., McManus, J.F., Robinson, L.F., 2014. $^{231}Pa/^{230}Th$ evidence for a weakened but persistent Atlantic meridional overturning circulation during Heinrich Stadial 1. Nat. Commun. 5, 5817. https://doi.org/10.1038/ncomms6817.

Broecker, W.S., Denton, G.H., 1990. The role of ocean-atmosphere reorganizations in glacial cycles. Quat. Sci. Rev. 9, 305–341. https://doi.org/10.1016/0277-3791(90)90026-7.

Caesar, L., Rahmstorf, S., Robinson, A., Feulner, G., Saba, V., 2018. Observed fingerprint of a weakening Atlantic Ocean overturning circulation. Nature 556, 191–196. https://doi.org/10.1038/s41586-018-0006-5.

Caesar, L., McCarthy, G.D., Thornalley, D.J.R., Cahill, N., Rahmstorf, S., 2021. Current atlantic meridional overturning circulation weakest in last millennium. Nat. Geosci. 14, 118–120. https://doi.org/10.1038/s41561-021-00699-z.

Channell, J., 2006. Late brunhes polarity excursions (mono lake, Laschamp, Iceland basin and pringle falls) recorded at ODP site 919 (irminger basin). Earth Planet Sci. Lett. 244, 378–393. https://doi.org/10.1016/j.epsl.2006.01.021.

Channell, J.E.T., Hodell, D.A., Lehman, B., 1997. Relative Geomagnetic Paleointensity and δ18O at ODP Site 983 Gardar Drift, North Atlantic/since 350 Ka, vol. 16.

Channell, J.E.T., Mazaud, A., Sullivan, P., Turner, S., Raymo, M.E., 2013. Rock magentic investigations of ODP Site 162–983. https://doi.org/10.1594/PANGAEA.808979.

Curry, W.B., Oppo, D.W., 2005. Glacial water mass geometry and the distribution of $\delta^{13}C$ of ΣCO_2 in the western Atlantic Ocean. Paleoceanography 20, 2004PA001021. https://doi.org/10.1029/2004PA001021.

Daniault, N., Mercier, H., Lherminier, P., Sarafanov, A., Falina, A., Zunino, P., Pérez, F.F., Ríos, A.F., Ferron, B., Huck, T., Thierry, V., Gladyshev, S., 2016. The northern North Atlantic Ocean mean circulation in the early 21st century. Prog. Oceanogr. 146, 142–158. https://doi.org/10.1016/j.pocean.2016.06.007.

Dansgaard, W., Johnsen, S.J., Clausen, H.B., Dahl-Jensen, D., Gundestrup, N.S., Hammer, C.U., Hvidberg, C.S., Steffensen, J.P., Sveinbjörnsdottir, A.E., Jouzel, J., Bond, G., 1993. Evidence for general instability of past climate from a 250-kyr ice-core record. Nature 364, 218–220. https://doi.org/10.1038/364218a0.

Davtian, N., Bard, E., 2023. A new view on abrupt climate changes and the bipolar seesaw based on paleotemperatures from Iberian Margin sediments. Proc. Natl. Acad. Sci. U.S.A. 120, e2209558120. https://doi.org/10.1073/pnas.2209558120.

Deaney, E.L., Barker, S., Van De Flierdt, T., 2017. Timing and nature of AMOC recovery across Termination 2 and magnitude of deglacial CO_2 change. Nat. Commun. 8, 14595. https://doi.org/10.1038/ncomms14595.

Dickson, R.R., Brown, J., 1994. The production of North Atlantic deep water: sources, rates, and pathways. J. Geophys. Res. 99, 12319. https://doi.org/10.1029/94JC00530.

Dokken, T.M., Nisancioglu, K.H., Li, C., Battisti, D.S., Kissel, C., 2013. Dansgaard-Oeschger cycles: interactions between ocean and sea ice intrinsic to the Nordic seas. Paleoceanography 28, 491–502. https://doi.org/10.1002/palo.20042.

Duplessy, J.C., Shackleton, N.J., Fairbanks, R.G., Labeyrie, L., Oppo, D., Kallel, N., 1988. Deepwater source variations during the last climatic cycle and their impact on the global deepwater circulation. Paleoceanography 3, 343–360. https://doi.org/10.1029/PA003i003p00343.

Eldevik, T., Nilsen, J.E.Ø., Iovino, D., Anders Olsson, K., Sandø, A.B., Drange, H., 2009. Observed sources and variability of Nordic seas overflow. Nat. Geosci. 2, 406–410. https://doi.org/10.1038/ngeo518.

Ellison, C.R.W., Chapman, M.R., Hall, I.R., 2006. Surface and deep ocean interactions during the cold climate event 8200 years ago. Science 312, 1929–1932. https://doi.org/10.1126/science.1127213.

Gherardi, J.M., Labeyrie, L., Nave, S., Francois, R., McManus, J.F., Cortijo, E., 2009. Glacial-interglacial circulation changes inferred from $^{231}Pa/^{230}Th$ sedimentary record in the North Atlantic region. Paleoceanography 24, 2008PA001696. https://doi.org/10.1029/2008PA001696.

Grützner, J., Higgins, S.M., 2010. Threshold behavior of millennial scale variability in deep water hydrography inferred from a 1.1 Ma long record of sediment provenance at the southern Gardar Drift: threshold behavior. Paleoceanography 25, 17. https://doi.org/10.1029/2009PA001873.

Hansen, B., Østerhus, S., 2000. North atlantic–nordic seas exchanges. Prog. Oceanogr. 45, 109–208. https://doi.org/10.1016/S0079-6611(99)00052-X.

Heaton, T.J., Köhler, P., Butzin, M., Bard, E., Reimer, R.W., Austin, W.E.N., Bronk Ramsey, C., Grootes, P.M., Hughen, K.A., Kromer, B., Reimer, P.J., Adkins, J., Burke, A., Cook, M.S., Olsen, J., Skinner, L.C., 2020. Marine20—the marine radiocarbon age calibration curve (0–55,000 cal BP). Radiocarbon 62, 779–820. https://doi.org/10.1017/RDC.2020.68.

Henry, L.G., McManus, J.F., Curry, W.B., Roberts, N.L., Piotrowski, A.M., Keigwin, L.D., 2016. North Atlantic ocean circulation and abrupt climate change during the last glaciation. Science 353, 470–474. https://doi.org/10.1126/science.aaf5529.

Hodell, D.A., Channell, J.E.T., Curtis, J.H., Romero, O.E., Röhl, U., 2008. Onset of "hudson strait" Heinrich events in the eastern North Atlantic at the end of the middle pleistocene transition (~640 ka)? Paleoceanography 23, 2008PA001591. https://doi.org/10.1029/2008PA001591.

Hodell, D., Lourens, L., Crowhurst, S., Konijnendijk, T., Tjallingii, R., Jiménez-Espejo, F., Skinner, L., Tzedakis, P.C., Abrantes, F., Acton, G.D., Alvarez Zarikian, Bahr, A., Balestra, B., Barranco, E.L., Carrara, G., Ducassou, E., Flood, R.D., Flores, J.-A., Furota, S., Grimalt, J., Grunert, P., Hernández-Molina, J., Kim, J.K., Krissek, L.A., Kuroda, J., Li, B., Lofi, J., Margari, V., Martrat, B., Miller, M.D., Nanayama, F., Nishida, N., Richter, C., Rodrigues, T., Rodríguez-Tovar, F.J., Roque, A.C.F., Sanchez Goñi, Sierro Sánchez, Singh, A.D., Sloss, C.R., Stow, D.A.V., Takashimizu, Y., Tzanova, A., Voelker, A., Xuan, C., Williams, T., 2015. A reference time scale for Site U1385 (Shackleton Site) on the SW Iberian Margin. Global and Planetary Change 133, 49–64. https://doi.org/10.1016/j.gloplacha.2015.07.002.

Hodell, D.A., Minth, E.K., Curtis, J.H., McCave, I.N., Hall, I.R., Channell, J.E.T., Xuan, C., 2009. Surface and deep-water hydrography on Gardar Drift (Iceland Basin) during the last interglacial period. Earth Planet Sci. Lett. 288, 10–19. https://doi.org/10.1016/j.epsl.2009.08.040.

Hodell, D.A., Crowhurst, S.J., Lourens, L., Margari, V., Nicolson, J., Rolfe, J.E., Skinner, L.C., Thomas, N.C., Tzedakis, P.C., Mleneck-Vautravers, M.J., Wolff, E.W., 2023. A 1.5-million-year record of orbital and millennial climate variability in the North Atlantic. Clim. Past 19, 607–636. https://doi.org/10.5194/cp-19-607-2023.

Howe, J.N.W., Piotrowski, A.M., Noble, T.L., Mulitza, S., Chiessi, C.M., Bayon, G., 2016. North Atlantic deep water production during the last glacial maximum. Nat. Commun. 7, 11765. https://doi.org/10.1038/ncomms11765.

Keigwin, L.D., Swift, S.A., 2017. Carbon isotope evidence for a northern source of deep water in the glacial western North Atlantic. Proc. Natl. Acad. Sci. U.S.A. 114, 2831–2835. https://doi.org/10.1073/pnas.1614693114.

Kissel, C., 2005. Magnetic signature of rapid climatic variations in glacial North Atlantic, a review. Compt. Rendus Geosci. 337, 908–918. https://doi.org/10.1016/j.crte.2005.04.009.

Kissel, C., Laj, C., Labeyrie, L., Dokken, T., Voelker, A., Blamart, D., 1999. Rapid climatic variations during marine isotopic stage 3: magnetic analysis of sediments from Nordic Seas and North Atlantic. Earth Planet Sci. Lett. 171, 489–502. https://doi.org/10.1016/S0012-821X(99)00162-4.

Kissel, C., Laj, C., Piotrowski, A.M., Goldstein, S.L., Hemming, S.R., 2008. Millennial-scale propagation of Atlantic deep waters to the glacial Southern Ocean. Paleoceanography 23, 2008PA001624. https://doi.org/10.1029/2008PA001624.

Kissel, C., Laj, C., Mulder, T., Wandres, C., Cremer, M., 2009. The magnetic fraction: a tracer of deep water circulation in the North Atlantic. Earth Planet Sci. Lett. 288, 444–454. https://doi.org/10.1016/j.epsl.2009.10.005.

Kissel, C., Van Toer, A., Laj, C., Cortijo, E., Michel, E., 2013. Variations in the strength of the North Atlantic bottom water during Holocene. Earth Planet Sci. Lett. 369–370, 248–259. https://doi.org/10.1016/j.epsl.2013.03.042.

Kleiven, H.F., Hall, I.R., McCave, I.N., Knorr, G., Jansen, E., 2011. Coupled deep-water flow and climate variability in the middle Pleistocene North Atlantic. Geology 39, 343–346. https://doi.org/10.1130/G31651.1.
Lacasse, C., Carey, S., Sigurdsson, H., 1998. Volcanogenic sedimentation in the Iceland Basin: influence of subaerial and subglacial eruptions. J. Volcanol. Geoth. Res. 83, 47–73. https://doi.org/10.1016/S0377-0273(98)00015-8.
Laj, C., 2003. MD 132/P.I.C.A.S.S.O.-IMAGES11 cruise, Marion Dufresne R/V. https://doi.org/10.17600/3200050.
Lamy, F., Winckler, G., Arz, H.W., Farmer, J.R., Gottschalk, J., Lembke-Jene, L., Middleton, J.L., Van Der Does, M., Tiedemann, R., Alvarez Zarikian, C., Basak, C., Brombacher, A., Dumm, L., Esper, O.M., Herbert, L.C., Iwasaki, S., Kreps, G., Lawson, V.J., Lo, L., Malinverno, E., Martinez-Garcia, A., Michel, E., Moretti, S., Moy, C.M., Ravelo, A.C., Riesselman, C.R., Saavedra-Pellitero, M., Sadatzki, H., Seo, I., Singh, R.K., Smith, R.A., Souza, A.L., Stoner, J.S., Toyos, M., De Oliveira, I.M. V.P., Wan, S., Wu, S., Zhao, X., 2024. Five million years of Antarctic Circumpolar Current strength variability. Nature 627, 789–796. https://doi.org/10.1038/s41586-024-07143-3.
Lascu, I., Feinberg, J.M., Dorale, J.A., Cheng, H., Edwards, R.L., 2016. Age of the Laschamp excursion determined by U-Th dating of a speleothem geomagnetic record from North America. Geology 44, 139–142. https://doi.org/10.1130/G37490.1.
Lisiecki, L.E., Raymo, M.E., 2005. A Pliocene-Pleistocene stack of 57 globally distributed benthic $\delta^{18}O$ records. Paleoceanography 20, 2004PA001071. https://doi.org/10.1029/2004PA001071.
Lougheed, B.C., Obrochta, S.P., 2019. A rapid, deterministic age-depth modeling routine for geological sequences with inherent depth uncertainty. Paleoceanogr. Paleoclimatol. 34, 122–133. https://doi.org/10.1029/2018PA003457.
Lynch-Stieglitz, J., 2017. The atlantic meridional overturning circulation and abrupt climate change. Ann. Rev. Mar. Sci 9, 83–104. https://doi.org/10.1146/annurev-marine-010816-060415.
Lynch-Stieglitz, J., Adkins, J.F., Curry, W.B., Dokken, T., Hall, I.R., Herguera, J.C., Hirschi, J.J.-M., Ivanova, E.V., Kissel, C., Marchal, O., Marchitto, T.M., McCave, I.N., McManus, J.F., Mulitza, S., Ninnemann, U., Peeters, F., Yu, E.-F., Zahn, R., 2007. Atlantic meridional overturning circulation during the last glacial maximum. Science 316, 66–69. https://doi.org/10.1126/science.1137127.
Martrat, B., Grimalt, J.O., Shackleton, N.J., De Abreu, L., Hutterli, M.A., Stocker, T.F., 2007. Four climate cycles of recurring deep and surface water destabilizations on the Iberian margin. Science 317, 502–507. https://doi.org/10.1126/science.1139994.
Mauritzen, C., 1996. Production of dense overflow waters feeding the North Atlantic across the Greenland-Scotland Ridge. Part 1: evidence for a revised circulation scheme. Deep Sea Res. Oceanogr. Res. Pap. 43, 769–806. https://doi.org/10.1016/0967-0637(96)00037-4.
Mazaud, A., Channell, J.E.T., Stoner, J.S., 2012. Relative paleointensity and environmental magnetism since 1.2Ma at IODP site U1305 (Eirik Drift, NW Atlantic). Earth and Planetary Science Letters 357–358, 137–144. https://doi.org/10.1016/j.epsl.2012.09.037.
McCave, I., Andrews, N, 2019. Distinguishing current effects in sediments delivered to the ocean by ice. I. Principles, methods and examples. Quaternary Science Reviews 212, 92–107. https://doi.org/10.1016/j.quascirev.2019.03.031.
McCave, I.N., Lonsdale, P.F., Hollister, Gardner, W.D., 1980. Sediment transport over the hatton and gardar contourite drifts. SEPM JSR 50, 1049–1062. https://doi.org/10.1306/212F7B76-2B24-11D7-8648000102C1865D.
McManus, J.F., Oppo, D.W., Cullen, J.L., 1999. A 0.5-million-year record of millennial-scale climate variability in the North Atlantic. Science 283, 971–975. https://doi.org/10.1126/science.283.5404.971.
McManus, J.F., Francois, R., Gherardi, J.-M., Keigwin, L.D., Brown-Leger, S., 2004. Collapse and rapid resumption of Atlantic meridional circulation linked to deglacial climate changes. Nature 428, 834–837. https://doi.org/10.1038/nature02494.
Moros, M., Endler, R., Lackschewitz, K.S., Wallrabe-Adams, H.-J., Mienert, J., Lemke, W., 1997. Physical properties of Reykjanes Ridge sediments and their linkage to high-resolution Greenland Ice Sheet Project 2 ice core data. Paleoceanography 12, 687–695. https://doi.org/10.1029/97PA02030.
Ng, H.C., Robinson, L.F., McManus, J.F., Mohamed, K.J., Jacobel, A.W., Ivanovic, R.F., Gregoire, L.J., Chen, T., 2018. Coherent deglacial changes in western Atlantic Ocean circulation. Nat. Commun. 9, 2947. https://doi.org/10.1038/s41467-018-05312-3.
Østerhus, S., Sherwin, T., Quadfasel, D., Hansen, B., 2008. The overflow transport East of Iceland. In: Dickson, R.R., Meincke, J., Rhines, P. (Eds.), Arctic–subarctic Ocean Fluxes: Defining the Role of the Northern Seas in Climate. Springer Netherlands, Dordrecht, pp. 427–441. https://doi.org/10.1007/978-1-4020-6774-7_19.
Paillard, D., Labeyrie, L., Yiou, P., 1996. Macintosh Program performs time-series analysis. EoS Transactions 77. https://doi.org/10.1029/96EO00259, 379–379.
Past Interglacials Working Group of PAGES, 2016. Interglacials of the last 800,000 years. Rev. Geophys. 54, 162–219. https://doi.org/10.1002/2015RG000482.
Paterson, G.A., Heslop, D., 2015. New methods for unmixing sediment grain size data. G-cubed 16, 4494–4506. https://doi.org/10.1002/2015GC006070.
Pöppelmeier, F., Jeltsch-Thömmes, A., Lippold, J., Joos, F., Stocker, T.F., 2023. Multi-proxy constraints on Atlantic circulation dynamics since the last ice age. Nat. Geosci. 16, 349–356. https://doi.org/10.1038/s41561-023-01140-3.
Rahmstorf, S., 2002. Ocean circulation and climate during the past 120,000 years. Nature 419, 207–214. https://doi.org/10.1038/nature01090.
Rasmussen, T.L., Thomsen, E., Van Weering, T.C.E., Labeyrie, L., 1996. Rapid changes in surface and deep water conditions at the Faeroe Margin during the last 58,000 years. Paleoceanography 11, 757–771. https://doi.org/10.1029/96PA02618.
Raymo, M.E., Oppo, D.W., Flower, B.P., Hodell, D.A., McManus, J.F., Venz, K.A., Kleiven, K.F., McIntyre, K., 2004. Stability of North Atlantic water masses in face of pronounced climate variability during the Pleistocene. Paleoceanography 19, 2003PA000921. https://doi.org/10.1029/2003PA000921.
Saunders, P.M., 1994. The flux of overflow water through the Charlie-Gibbs Fracture Zone. J. Geophys. Res. 99, 12343. https://doi.org/10.1029/94JC00527.
Sigmarsson, O., Maclennan, J., Carpentier, M., 2008. Geochemistry of igneous rocks in Iceland: a review. Jök 58, 139–160. https://doi.org/10.33799/jokull2008.58.139.
Stevenard, N., Govin, A., Kissel, C., Van Toer, A., 2023. Correction of the IRD influence for paleo-current flow speed reconstructions in hemipelagic sediments. Paleoceanogr. Paleoclimatol. 38, e2022PA004500. https://doi.org/10.1029/2022PA004500.
Süfke, F., Pöppelmeier, F., Goepfert, T.J., Regelous, M., Koutsodendris, A., Blaser, P., Gutjahr, M., Lippold, J., 2019. Constraints on the Northwestern Atlantic deep water circulation from $^{231}Pa/^{230}Th$ during the last 30,000 years. Paleoceanogr. Paleoclimatol. 34, 1945–1958. https://doi.org/10.1029/2019PA003737.
Thornalley, D.J.R., Blaschek, M., Davies, F.J., Praetorius, S., Oppo, D.W., McManus, J.F., Hall, I.R., Kleiven, H., Renssen, H., McCave, I.N., 2013. Long-term variations in Iceland–Scotland overflow strength during the Holocene. Clim. Past 9, 2073–2084. https://doi.org/10.5194/cp-9-2073-2013.
Toucanne, S., Soulet, G., Vázquez Riveiros, N., Boswell, S.M., Dennielou, B., Waelbroeck, C., Bayon, G., Mojtahid, M., Bosq, M., Sabine, M., Zaragosi, S., Bourillet, J., Mercier, H., 2021. The North Atlantic glacial Eastern Boundary Current as a key driver for ice-sheet—AMOC interactions and climate instability. Paleoceanogr. Paleoclimatol. 36, e2020PA004068. https://doi.org/10.1029/2020PA004068.
Toyos, M.H., Lamy, F., Lange, C.B., Lembke-Jene, L., Saavedra-Pellitero, M., Esper, O., Arz, H.W., 2020. Antarctic circumpolar current dynamics at the pacific entrance to the drake passage over the past 1.3 million years. Paleoceanogr. Paleoclimatol. 35, e2019PA003773. https://doi.org/10.1029/2019PA003773.
Tzedakis, P.C., Raynaud, D., McManus, J.F., Berger, A., Brovkin, V., Kiefer, T., 2009. Interglacial diversity. Nat. Geosci. 2, 751–755. https://doi.org/10.1038/ngeo660.
Veres, D., Bazin, L., Landais, A., Toyé Mahamadou Kele, H., Lemieux-Dudon, B., Parrenin, F., Martinerie, P., Blayo, E., Blunier, T., Capron, E., Chappellaz, J., Rasmussen, S.O., Severi, M., Svensson, A., Vinther, B., Wolff, E.W., 2013. The Antarctic ice core chronology (AICC2012): an optimized multi-parameter and multi-site dating approach for the last 120 thousand years. Clim. Past 9, 1733–1748. https://doi.org/10.5194/cp-9-1733-2013.
Wary, M., Eynaud, F., Swingedouw, D., Masson-Delmotte, V., Matthiessen, J., Kissel, C., Zumaque, J., Rossignol, L., Jouzel, J., 2017. Regional seesaw between the North Atlantic and Nordic Seas during the last glacial abrupt climate events. Clim. Past 13, 729–739. https://doi.org/10.5194/cp-13-729-2017.
Weeks, R., Laj, C., Endignoux, L., Fuller, M., Roberts, A., Manganne, R., Blanchard, E., Goree, W., 1993. Improvements in long-core measurement techniques: applications in palaeomagnetism and palaeoceanography. Geophys. J. Int. 114, 651–662. https://doi.org/10.1111/j.1365-246X.1993.tb06994.x.
Weltje, G.J., Tjallingii, R., 2008. Calibration of XRF core scanners for quantitative geochemical logging of sediment cores: theory and application. Earth Planet Sci. Lett. 274, 423–438. https://doi.org/10.1016/j.epsl.2008.07.054.
Weltje, G.J., Bloemsma, M.R., Tjallingii, R., Heslop, D., Röhl, U., Croudace, I.W., 2015. Prediction of geochemical composition from XRF core scanner data: a new multivariate approach including automatic selection of calibration samples and quantification of uncertainties, in: micro-XRF studies of sediment cores. In: Croudace, I.W., Rothwell, R.G. (Eds.), Developments in Paleoenvironmental Research, vol. 17. Springer Netherlands, Dordrecht, pp. 507–534. https://doi.org/10.1007/978-94-017-9849-5_21.
Wu, L., Wilson, D.J., Wang, R., Yin, X., Chen, Z., Xiao, W., Huang, M., 2020. Evaluating Zr/Rb ratio from XRF scanning as an indicator of grain-size variations of glaciomarine sediments in the Southern Ocean. G-cubed 21, e2020GC009350. https://doi.org/10.1029/2020GC009350.
McCave, I.N., 2007. Chapter one: Deep-sea sediment deposits and properties controlled by currents, in: Developments in marine geology, vol. 1. Elsevier,, pp. 19–62. https://doi.org/10.1016/S1572-5480(07)01006-8.